


Interaction Notes

Note 630

6 November 2019

Direct-Strike Lightning Response Estimates of Buried Cables within a Communication Facility

Dr. F.M. Tesche
 Consultant (Retired)

Dr. D. V. Giri
Pro-Tech, Wellesley, MA 02481
Dept. of ECE, University of New Mexico

and

Dr. Armin Kaelin
Formerly with armasuisse, now with EMProtec GmbH, Switzerland

Abstract

This note examines the responses of four different types of shielded cables to a direct lightning strike. The cables are buried in the ground and run between two shielded enclosures, one of which is struck by lightning. An induced current flows on the cable shield and this induces a voltage on the inner conductors within the shield. Using several different models, this voltage is estimated and the effectiveness of the various shields is determined. From this study, requirements for lightning surge protection devices can be developed for this system.

1. Introduction

Naturally occurring lightning often poses a severe threat to modern electronics equipment. Successively smaller and more sensitive electrical components may suffer logic upset or permanent damage at induced signal levels that, in the past, had been considered safe. As a result, there is considerable interest in estimating the possible range of lightning-induced surges within shielded enclosures containing advanced electronics.

This note documents a study undertaken to evaluate the lightning-induced voltages on shielded signal or power cables within a protected building. The configuration of the problem of interest is illustrated in Figure 1. A well-protected building (similar in construction to a Faraday cage) is located in a prominent position that is susceptible to direct lightning strikes. This building has communication antennas, together with other appendages that attract the lightning. It is this current surge that may adversely affect internal equipment within the building.

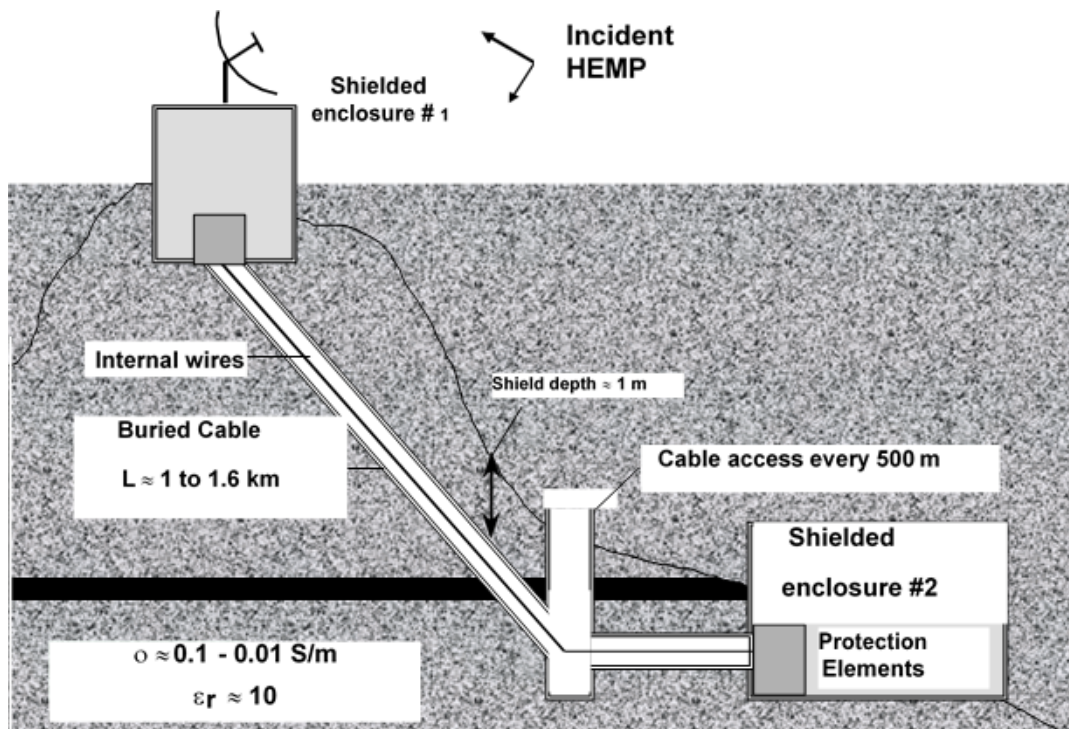


Figure 1. Illustration of two shielded enclosures connected by a buried, shielded cable and excited by a direct lightning strike.

In this system, a buried cable containing power or signal lines exits the building. This cable forms an electromagnetic (EM) field that reduces the pickup of the lightning current by the internal wires. The cable can extend for distances approaching 1 to 1.6 km, at which point it is connected to another shielded enclosure, also containing electronic equipment. Occasional access hatches for cable connection and maintenance may be found every 300 to 500 meters along the length of the cable run.

Given this system geometry, the goal of the present study is to estimate the lightning-induced voltage surges on the internal shielded wires as they enter the second enclosure. Knowing the levels of typical responses will permit the specification and design of the surge protection devices needed at the equipment in the system. These responses can be estimated using the idealized system model illustrated in Figure 2. In this model, the earth is modeled by a locally flat, imperfectly conducting material having an electrical conductivity σ , and the shielded cable is modeled as a buried cylindrical tube of length L buried in the soil at a depth d . The two enclosures are assumed to have an earthing (i.e., footing) resistance of R_1 and $R_3 \Omega$ with respect to a reference potential plane deep within the earth, with these parameters being dependent on the enclosure size and the earth conductivity. Additional details of these resistances will be presented in Section 3.2.

The lightning strike is assumed to occur at one of the enclosures, as illustrated in the figure. This lightning current splits, with part flowing to the earth reference point through the resistor R_1 and the remainder flowing out along the outer surface of the shielded cable. A fraction of this latter current leaks off into the soil, and the remainder flows over the second enclosure to ground through the resistance R_3 . In this model, the effects of the cable access hatches are neglected and the lightning current injected onto the structure is assumed to occur only at the enclosure. It can be shown that both of these assumptions lead to an overprediction of the responses, thereby giving an upper bound solution for the responses.

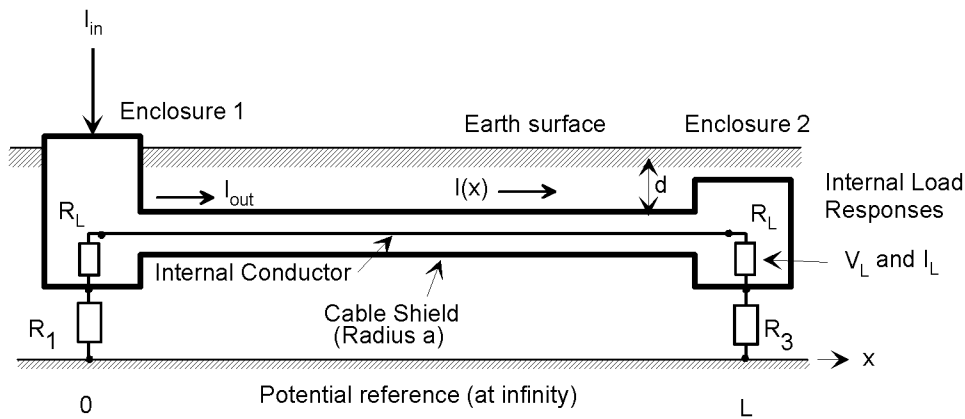
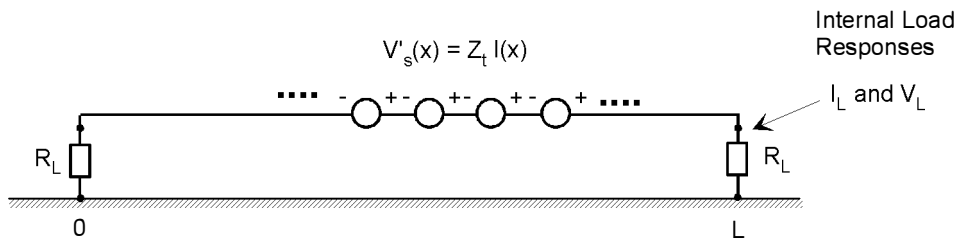


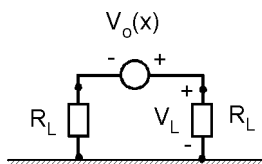
Figure 2. Detailed cable model of the shield and internal wire excited by a direct lightning strike.

In the model of the cable system in Figure 2, the desired response is the induced voltage across one of the internal load resistances within the cable shield, denoted by R_L . As will be discussed in Section 4, this response can be calculated from a knowledge of the external current on the cable shield $I(x)$, together with a shield parameter called the shield transfer impedance $Z_t(\omega)$. This model leads to a very simple distributed electrical circuit for

the transmission line within the cable shield, as shown in Figure 3a.. As will be seen later, the lightning current varies so slowly that the voltage sources in the distributed circuit can be lumped together as one source, and a simple lumped circuit may be used to represent the internal signal wires excited by the lightning current. This is illustrated in Figure 3b.



(a) Distributed circuit



(b) Lumped circuit

Figure 3. Circuit diagrams for evaluating the internal conductor voltage due to a direct lightning strike.

In this note, a numerical study of the response of the system of Figure 1 is described. Section 2 discusses nature of the assumed lightning current that induces current on the long buried cable shield, and various models for computing this current division on the structure are discussed in Section 3.

Section 4 continues with the development of the system model illustrated in Figure 2 for estimating the internal load response voltages at the equipment, given the external shield current. Using this model, various response levels are calculated for four different types of cable shields, and these results are summarized in Section 5. Finally, Section 6 concludes with a brief summary of the important results of the study.

2. The Lightning Environment

The first step in conducting this analysis is to develop an estimate of the lightning current that is injected onto the exterior of the protective enclosure. Significant work in this area has been reported, and like the high altitude electromagnetic pulse (HEMP) environment[†], there is no one universally accepted specification for the current that flows in a cloud-to-ground discharge. This is due to the fact that there can be large variations in observed lightning current waveforms.

A common approach taken in characterizing the lightning is to use a statistical representation for the probabilities of occurrence of important waveform parameters, such as the peak current and the maximum rate of rise. As an example, Figure 4 illustrates the cumulative probability distributions for the peak current of the first and subsequent lightning strikes to ground. We note that only about 10% of the observed first strikes will *exceed* a peak value of 50 kA, which is a commonly used value for a lightning stroke.

Similarly, Figure 5 illustrates the statistics for the peak rate of rise of the lightning current (in kA/ μ s) for the first and subsequent strokes. Note that in this simple view of the lightning environment, the data presented in Figure 4 and Figure 5 are taken to be independent. In reality, however, there is a correlation between the lightning peak value and rate of rise, and a more sophisticated statistical analysis is needed to account for this correlation.

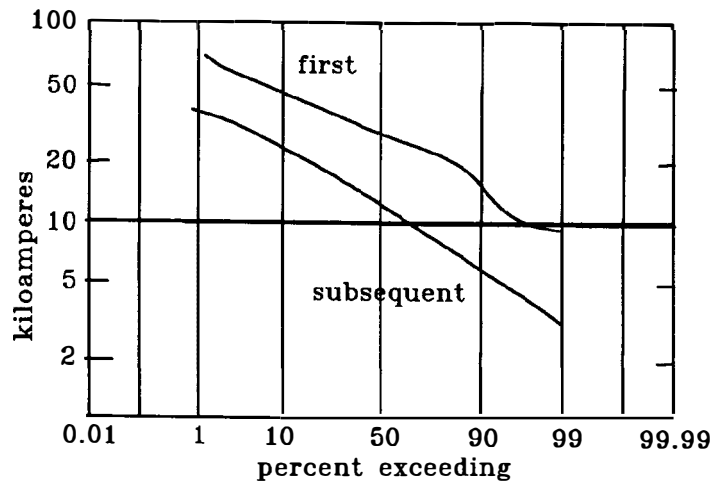


Figure 4. Statistics of the peak currents for the first and subsequent cloud-to-ground lightning strikes (from [1].)

[†] The HEMP responses of the same structure treated here are discussed in another companion Interaction Note 631.

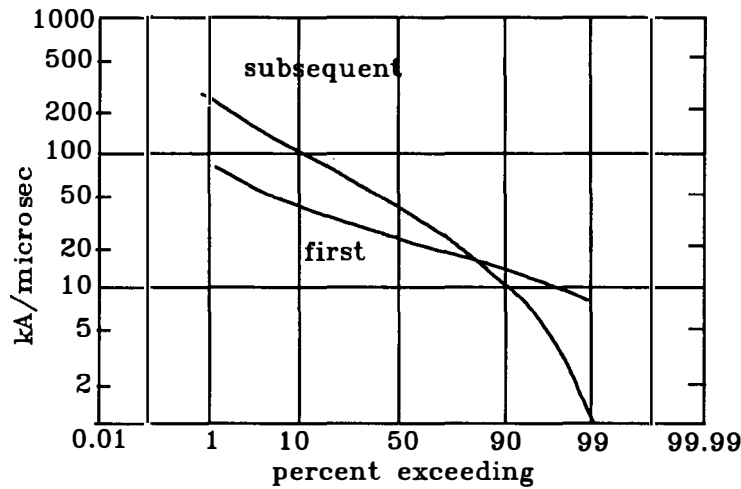


Figure 5. Statistics of the peak rate of rise of the current for the first and subsequent cloud-to-ground lightning strikes (from [1].)

It is useful to summarize the first-strike statistics of the lightning waveform in terms of a “severity level” of the strike. By defining the severity level as the *complement* of the “percent exceeding” values of Figure 4 and Figure 5, the data may be expressed as a percentage of strikes that are *lower* than the specified value. That is to say, a strike with a severity level of 90% will be such that 90% of all strikes will have a lower amplitude (or rate of rise), and 10% of all strikes will have a larger response. The first-strike statistical data in these figures are presented in Table 1.

Table 1. Peak lightning currents and rates of rise for different severity levels for a direct lightning strike.

Parameter	Severity Level						
	1 %	5%	10%	50%	90%	95%	99%
Peak Current (kA)	9	10	17	20	50	55	70
dI/dt (kA/ms)	8	10	13	20	25	50	80

Based on these and other measurements, several different specifications of lightning channel current have been published. For example, ref.[2] postulates the relatively simple waveform shown in Figure 6, which according to [1], has been used in the design of the Space Shuttle. This waveform has a peak amplitude of 50 kA and a peak derivative of 25 kA/μs, which provides a lightning current at severity level of about 90%.

The spectral response magnitude of this transient lightning current is illustrated in Figure 7, and it contains significant components up to approximately 10 kHz. In reality, the actual lightning spectrum will have significant high frequency components, but this is not evident from this postulated waveform due to its very simple early-time behavior.

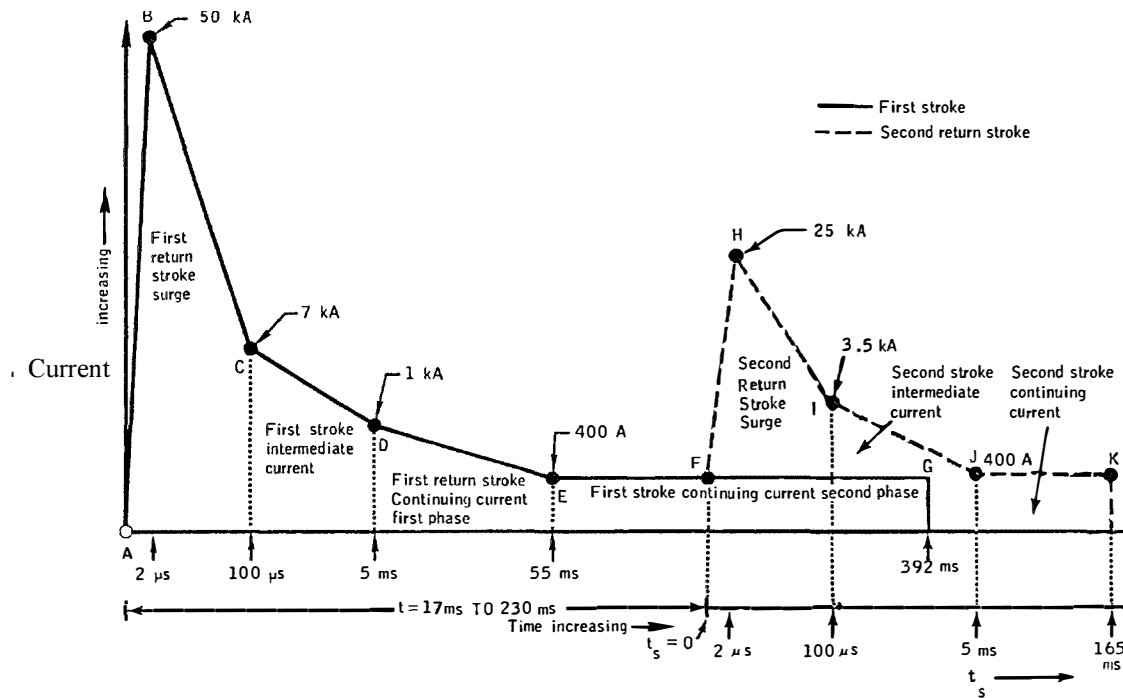


Figure 6. Lightning current specification used for the Space Shuttle (from [1]).

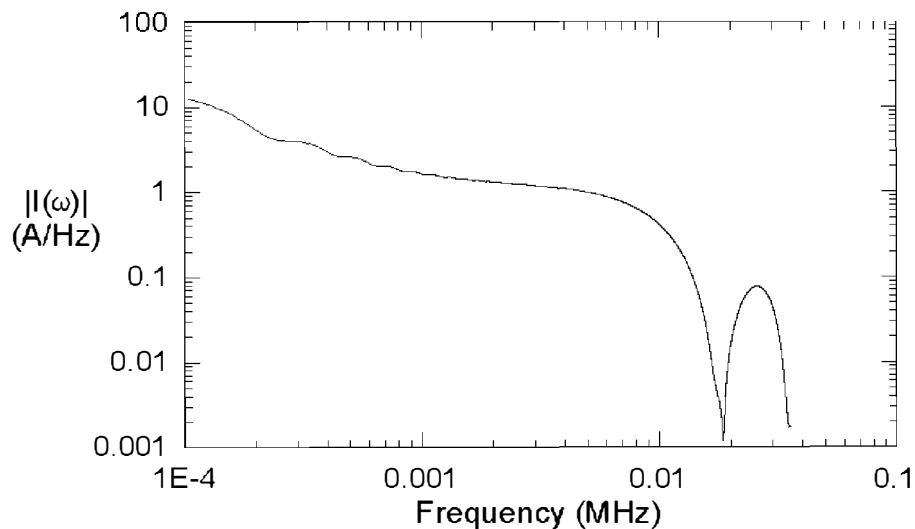


Figure 7. Spectral amplitude for the lightning current of Figure 6.

Note that other lightning current specifications are possible. Appendix A discusses a commonly used environment for computing the radiated EM field responses of transmission lines near a lightning channel. This alternate lightning waveform has a significantly lower peak value than the more stressing waveform shown in Figure 6. In fact, a comparison of the peak value of 12 kA of this waveform shows that about 92% of all lightning discharges will be expected to have a current *larger* than this level. As a consequence, for determining reasonable worst-case estimates of lightning responses of buildings and cables, the 50 kA lightning environment will be used.

3. Interaction of Lightning with Building and Cables

Given the assumed lightning current waveform of Figure 6, it is necessary to estimate how this current flows over the building and onto the buried cable. As shown in Figure 1, this cable runs away from the building and it is assumed to be at a fixed depth in the ground.

For simplicity, we will assume that the building is a good conductor, due to its rebar construction or to other shielding measures applied during its construction, and that the cable shield is electrically connected to the building enclosure. (This is the normal practice for constructing well-shielded systems.) The lightning strike provides an injected current onto the building, and it spreads over the building exterior in a search for a path to ground. As the current reaches the foundation of the building, it sees two possible paths: one from the building directly into the soil, and another from the building onto the long cable.

To estimate this current splitting and to find the current flowing on the buried cable, two approaches can be taken. The first involves an early-time model, in which the wavefront of the lightning current is tracked as it propagates down the channel and onto the enclosure, shielded cable, and the earth. This provides an indication of the very early-time response of the current, and is most useful for estimating the penetration of electromagnetic (EM) fields associated with the current into apertures or holes in the enclosures.

The second approach is a late-time calculation that examines the current splitting based on low frequency circuit models using resistive splitting networks. In this model, any early-time information contained in the waveform is eliminated and the resulting coupling response models are rather simple. This latter method, however, is most useful in examining the effects of the slow current diffusion through cable shields. Both of these analysis approaches are described in this section.

3.1 Early Time Responses

For the early-time response calculation for current flowing onto the cable shield, the geometry illustrated in Figure 8 is considered. Only the enclosure being struck and a long buried cable are considered; the other building is assumed to be too far away to influence the early-time responses.

The lightning channel current is denoted by I_{source} in this figure and to describe the cable current, the current ratio I_{source}/I_{out} is calculated. Once this current splitting factor is determined, the previously specified lightning current can be used to estimate the actual value of the transient current flowing onto the cable shield.

The calculation of the current splitting is a complicated problem, given the geometry of the partially buried enclosure and the time history of the excitation. One possible analysis approach is to use the finite difference time domain (FDTD) method [3] to solve for the time dependent E and H fields around the channel, enclosure and cable. This method divides the 3-dimensional space around the conductors into a finite mesh, and then time-steps the resulting difference equations representing Maxwell's equations to yield a transient solution. Because the time steps must be sufficiently small to resolve each cell in the mesh, this is inherently an "early time" analysis.

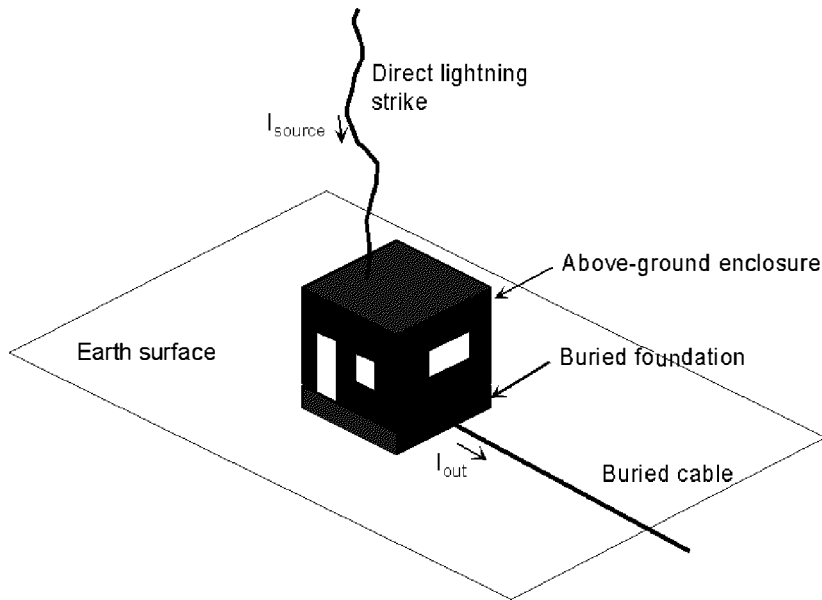


Figure 8. Illustration of a direct lightning strike on a building with a buried, shielded cable.

As an example of this procedure, consider a typical building with floor dimensions 3×4 meters and a height of 3 meters. The region surrounding the building, cable and channel is filled with a $61 \times 61 \times 101$ finite difference mesh, as shown in Figure 9. With the dimensions of the unit cells set to $\Delta x = \Delta y = \Delta z = 0.29$ meters, the resulting time step for these FDTD calculations is $\Delta t \approx 0.56$ ns. To adequately sample the lightning waveform (assumed to be about 100 ns long) would require on the order of 180 million time steps—clearly beyond the realm of possibility of present computers. Thus, while the FDTD calculation cannot be used to answer questions about the *late-time* interactions of the lightning with the building and cable, it can be used to study the *early-time* attachment of the channel to the roof and the initiation of the current splitting process.

To this end, a FDTD simulation of the lightning interaction was undertaken. A long, perfectly conducting lightning channel of radius 10 cm was run vertically from the center point of the enclosure roof as shown in Figure 9. Along this conductor, a transient voltage source supplying a Gaussian waveform was located at cell 36 directly above the building. The enclosure was assumed to have a foundation depth of approximately 0.9 meters, and the buried cable was at a depth of 0.6 meters. The electrical conductivity of the ground was 0.01 S/m and the cable radius was assumed to be 10 cm.

While the FDTD calculation is conducted using the E and H fields in the mesh, currents on the wires can be computed by integrating the H-field around a closed contour surrounding the wire [3]. This permits the estimate of the current flowing onto the enclosure and away from it on the buried cable. As an example of the behavior of the computed lightning channel current, Figure 10 presents a surface plot of the current, with time on the x-axis and the channel location along the y-axis. The vertical z-axis indicates the strength of the current.

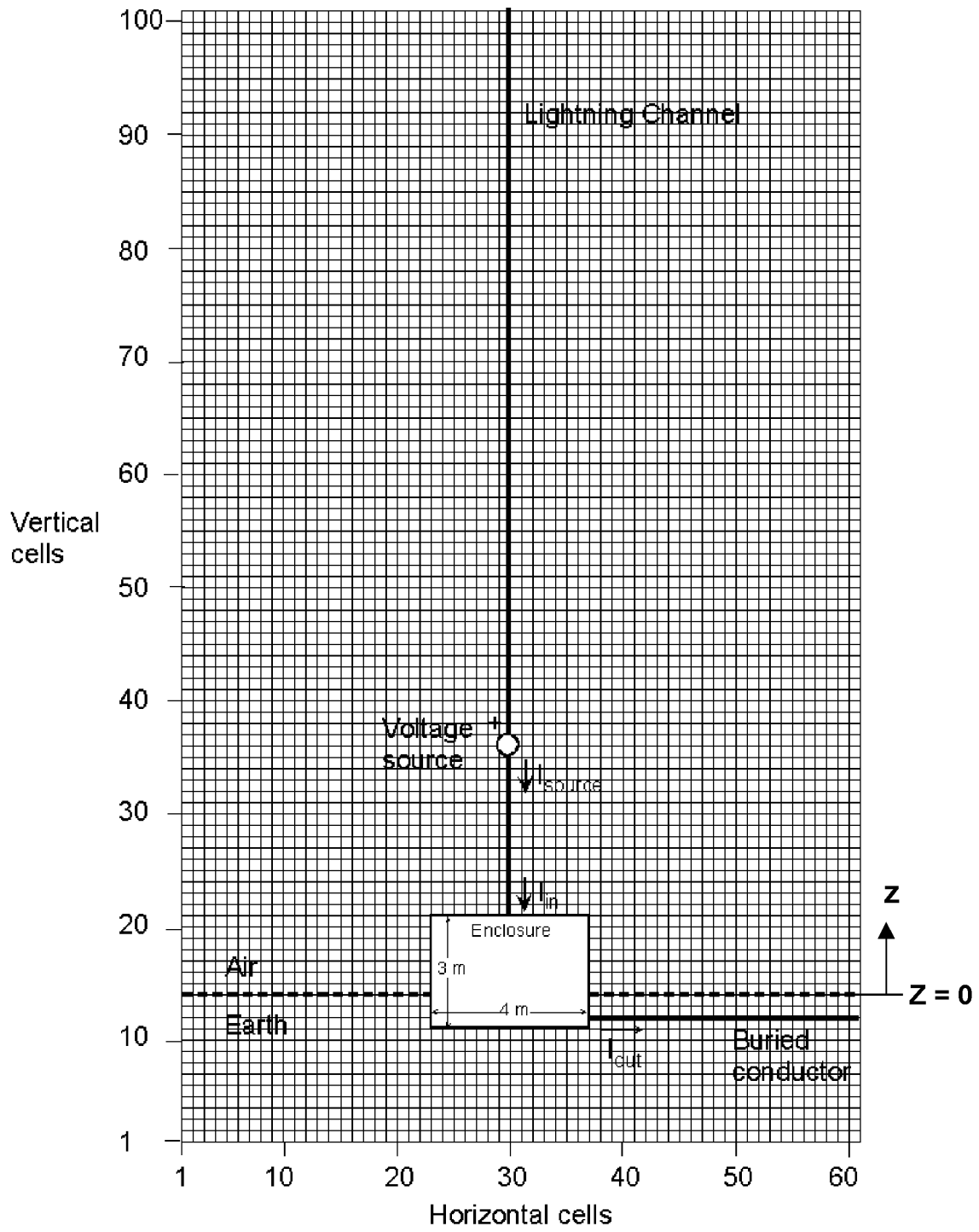


Figure 9. Side view of the $61 \times 61 \times 101$ mesh surrounding the building for the FDTD calculation.

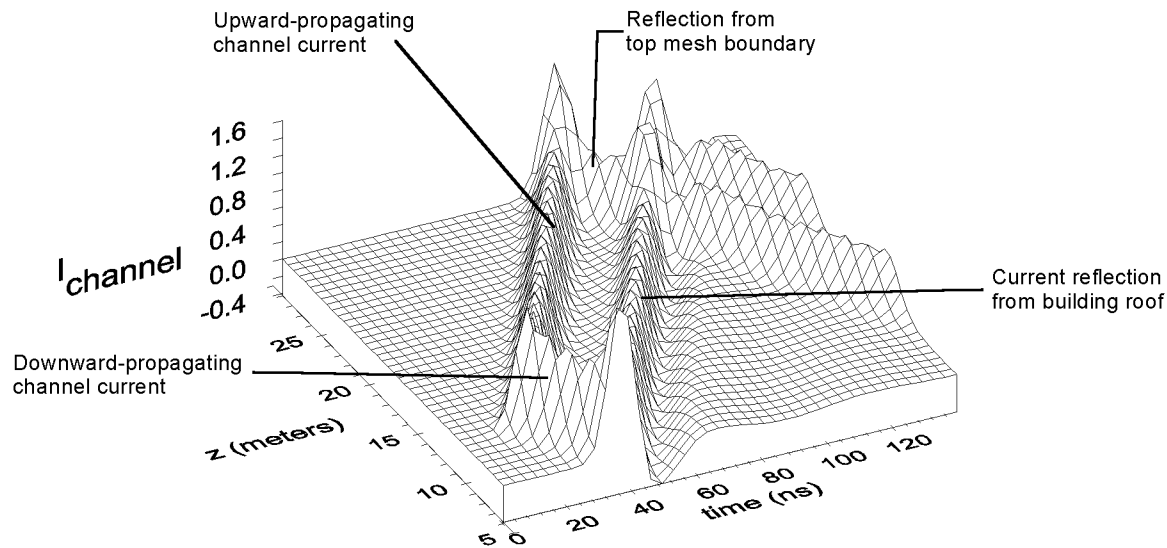


Figure 10. Surface plot of the unit-amplitude transient current along the lightning channel due to the Gaussian voltage source excitation at cell 35.

When the source is pulsed, it sends a downward-propagating pulse I_{source} towards the building, along with an upward propagating pulse along the channel with the same polarity. The strength of the voltage source has been adjusted so that the amplitude of the downward-propagating current wave is unity. As the channel current reaches the building, it suffers a reflection, which appears like that of a partially short circuit. It is not a perfect short, however, as evidenced by the fact that the current at the building attachment point is not exactly 2 times higher than the channel traveling wave.

The upward propagating pulse on the lightning channel eventually reaches the end of the computational grid and is reflected back to the building. When this reflected wave finally reaches the building, this unphysical artifact of the FDTD calculation corrupts the actual lightning response, and the simulation must end. This occurs at a time of roughly 150 ns.

From the family of waveforms comprising Figure 10, the individual transient waveforms for the channel current at the source, I_{source} , and the current injected onto the building, I_{in} , can be extracted. These are shown in Figure 11 and Figure 12, respectively. From the same FDTD calculation, the current flowing onto the cable, I_{out} , has been calculated and is shown in Figure 13.

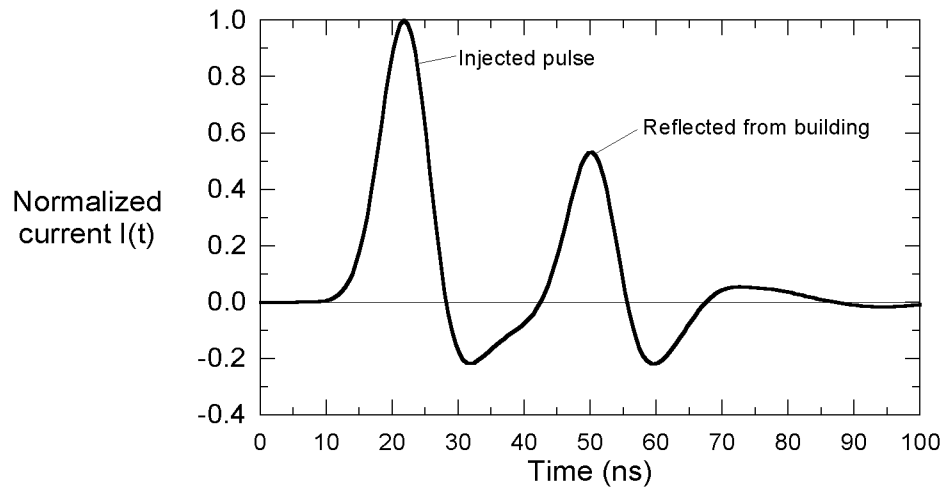


Figure 11. Plot of the transient current I_{source} at cell 34 just below the voltage source.

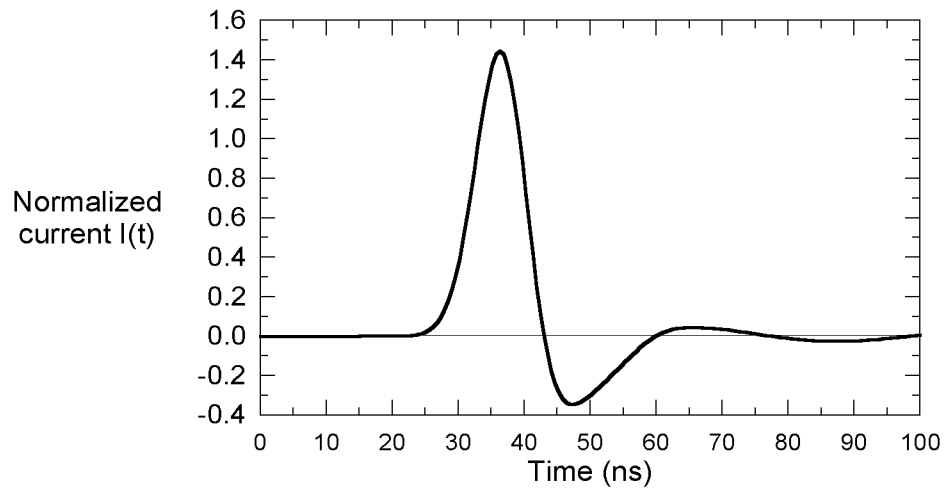


Figure 12. Plot of the transient current I_{in} at the top of the enclosure.

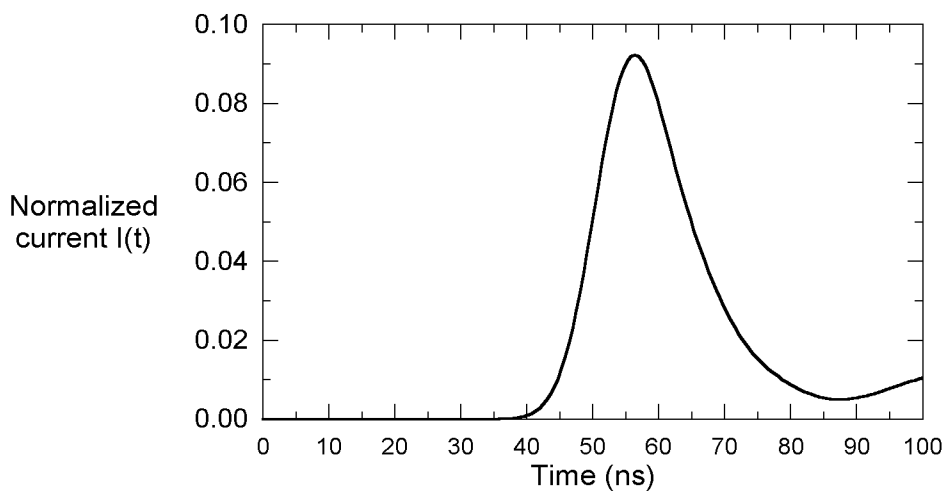


Figure 13. Plot of the transient current I_{out} flowing onto the buried cable.

3.2 Late Time Responses

From the early-time current transient responses using FDTD, we note that the fraction of lightning current injected onto the cable shield is given by the current splitting ratio $I_{out}/I_{source} \approx 0.1$. Thus, approximately 10% of the early-time lightning channel current will excite the cable shield. At later times, however, we expect that this ratio will change and will be affected by the length of the cable. At very late times, the lightning current division is governed by the dc footing (or “earthing”) resistance of both the buildings and the cable. An analysis of this case can be conducted using the various resistance models developed in [4].

Figure 14 illustrates a simple footing resistance model for the building and line geometry of Figure 2. The buried foundation of the building experiencing the direct lightning strike is approximated by a hemisphere of radius r , and this structure has a footing resistance in the soil given in [4] as

$$R_1 \approx \frac{1}{2\pi\sigma r} \text{ } (\Omega). \quad (1)$$

R_3 denotes the footing resistance of the second building (if the building is present). Assuming that the buildings are identical and the ground is homogeneous, we note that $R_3 = R_1$. Of course, in the real situation, the ground conductivity may be different at the two building sites, so this assumption may not be valid in all cases.

The buried cable of length L and radius a may be modeled by a horizontal conductor segment at a depth d . Assuming that this cable is in direct electrical contact with the soil, the resistance of this conductor is given by the expressions in [5] as

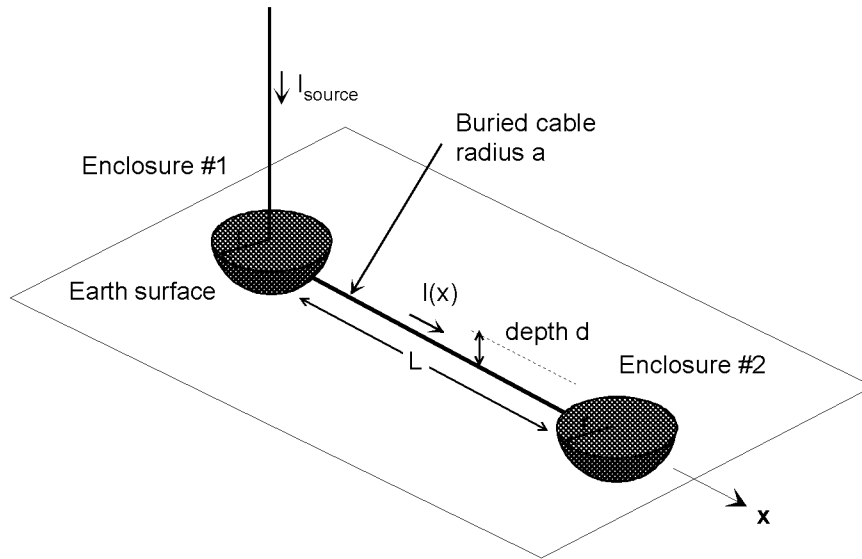
$$R_2 \approx \frac{1}{\pi\sigma L} \left[\ln\left(\frac{2L}{\sqrt{2ad}}\right) - 1 \right] \text{ } (\Omega) \text{ } (\text{for } d \ll L) \quad (2a)$$

or by

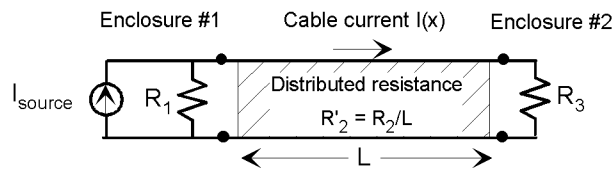
$$R_2 \approx \frac{1}{\pi\sigma L} \left[\ln\left(\frac{2L}{a}\right) - 1 \right] \text{ } (\Omega) \text{ } (\text{for } d = 0) \quad (2b)$$

for the cable lying directly on the surface of the earth. These expressions neglect mutual interactions between the buildings and this cable

Using these models, the simple distributed resistive circuit illustrated in Figure 14b can be used to estimate the lightning current on the cable. This current, denoted by $I(x)$, is a function of position along the cable, because a portion of the current leaks away from the cable into the earth, as suggested by Figure 15.



(a) Idealized building and cable geometry



(b) Distributed resistive circuit model

Figure 14. Low-frequency model of the footing resistance of the building and cable.

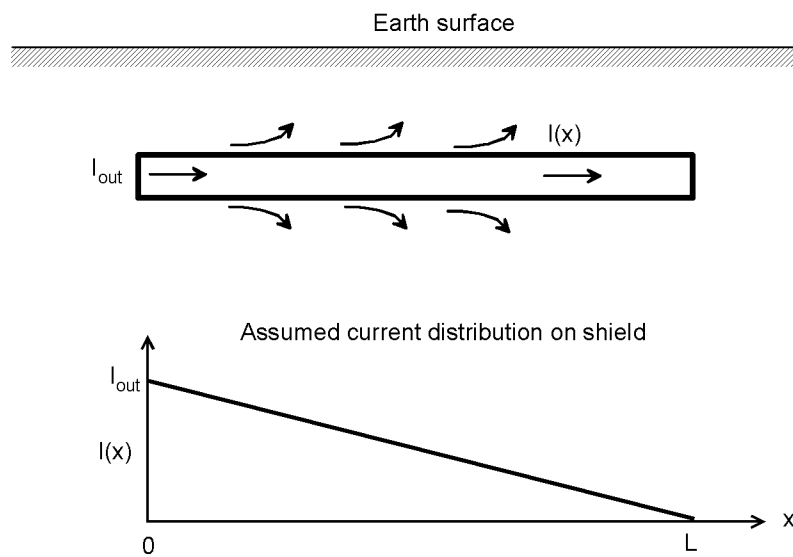


Figure 15. Illustration of current leaking from the buried shield into the soil.

A simple DC circuit analysis of the distributed circuit in Figure 14b yields the following expression for the cable shield current distribution:

$$I(x) = I_{source} \left(1 - \frac{G_1 + G_2 x / L}{G_1 + G_2 + G_3} \right) \quad (3)$$

where $G_1 = 1/R_1$, $G_2 = 1/R_2$ and $G_3 = 1/R_3$.

As will be discussed later in Section 4, the low frequency excitation of internal signal wires depends on the *average* current flowing over the shield. From Eq.(3), this average current on the shield is given simply as the current at the shield midpoint, or

$$I_{avg} = I_{source} \left(\frac{G_2 / 2 + G_3}{G_1 + G_2 + G_3} \right). \quad (4)$$

For the assumed case where $R_1 = R_3$, Eq.(4) becomes

$$\begin{aligned} I_{avg} &= I_{source} \left(\frac{G_2 / 2 + G_1}{2G_1 + G_2} \right) \\ &= 0.5 I_{source} \end{aligned} \quad (5)$$

This interesting result indicates that for the geometry shown in Figure 14a, the current splitting between the source current and the average cable current is *independent* of the soil conductivity and the details of the individual footing resistances.

Another useful case to consider is when enclosure #2 is not present and the cable shield at the $x = L$ end is effectively open-circuited. In this case, $G_3 = 1/R_3 = 0$ and the average current on the cable shield is given by

$$I_{avg} = \frac{1}{2} I_{source} \left(\frac{G_2}{G_1 + G_2} \right), \quad (6)$$

Notice that because the term G_2 depends on the length L via Eq.(2), the average shield current now depends on this length.

Buried cables often will have an insulation jacket surrounding the metal portion of the shield. At low current excitation levels, this jacket provides an effective barrier to the leakage current, with the result that $G_2 = 1/R_2 = 0$. In this case, Eq.(4) again gives the result that $I_{avg} = \frac{1}{2} I_{source}$ if $R_1 = R_3$. At the higher excitation levels expected in a lightning strike, however, the induced voltage across this insulating jacket can exceed several MV and this will cause a dielectric breakdown in the insulation. This results in a localized current flow from the cable into the soil.

Since the worst case internal response occurs when the external shield current is maximum, we note that the localized dielectric breakdown in the insulation will tend to *reduce* this response. Consequently, the worst-case response will occur when we assume either that *no* dielectric breakdown occurs (i.e., $G_2 = 1/R_2 = 0$), or that complete breakdown has occurred ($G_2 =$ uniformly distributed along the line), in which for both cases, the

average shield current is $I_{avg} = \frac{1}{2} I_{source}$. In the analysis that follows, we will examine assume that complete breakdown has occurred, and that the cable appears like an uninsulated conductor in direct contact with the soil. The case of isolated cable breakdowns is beyond the scope of this preliminary analysis, and may be considered in the future.

To illustrate the behavior of the late-time lightning current flowing onto the cable, Figure 16 plots the current splitting fraction $f = I_{avg}/I_{source}$ as a function of the cable length L for different burial depths d . For this plot the cable radius is $a = 10$ cm. This plot considers the two system configurations mentioned above – one in which there are identical buildings at each end of the cable, and another in which the cable extends out from the building at $x = 0$, with no building at $x = L$. This represents the case when the equipment enclosure at $x = L$ is much smaller than the first building.

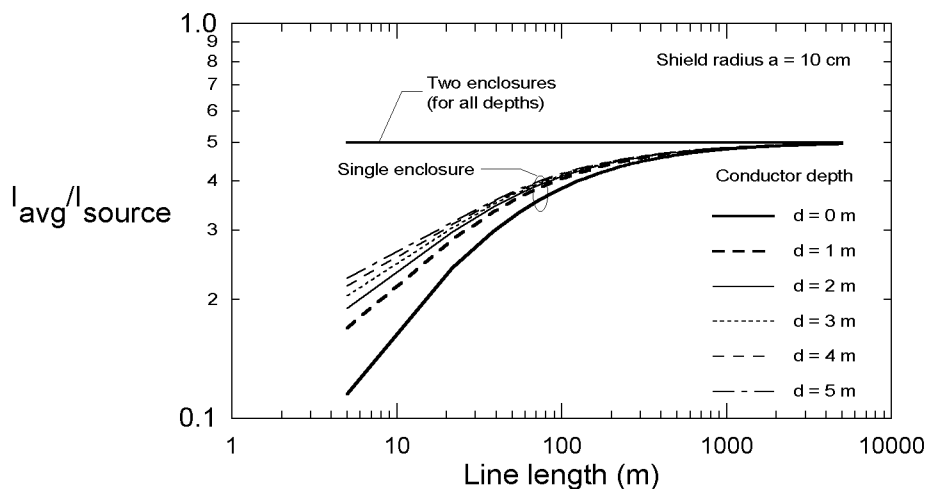


Figure 16. Plot of the average value of the late-time lightning current flowing onto the cable for a cable radius of 10 cm.

For the case of two identical buildings, we note from Eq.(5) that the current splitting fraction is independent of the cable length L . For the second case where the enclosure at $x = L$ is absent, the average current flowing on the cable is seen to be a function of the cable length. For very short cables, an order of magnitude reduction of the average shield current is possible. Notice that as the cable gets longer, more current flows on the cable due to the decreasing footing resistance, and eventually the average value of the shield current reaches $\frac{1}{2}$ of the injected lightning current. Also note that this current splitting is independent of the earth conductivity, as seen from Eq.(5).

Figure 17 and Figure 18 show the similar results for cables of radii 5 cm and 1 cm. It is interesting to compare the results of this current splitting with the early-time value of 10% that was determined previously. At very early times, the current transients on the building and cable have no way of knowing the length of the buried cable or any other details of how the cable is terminated. All current splitting is determined by the localized interaction of the building, cable and earth. From the data presented in Figure 16 through Figure 18, we note that for very short lines (say several meters in length) the current splitting fraction becomes small, say on the order of 0.1 – 0.2, and is consistent with that computed by the FDTD model. Longer cables, however, exhibit a much smaller current splitting ratio, with the value of 0.5 being the upper bound.

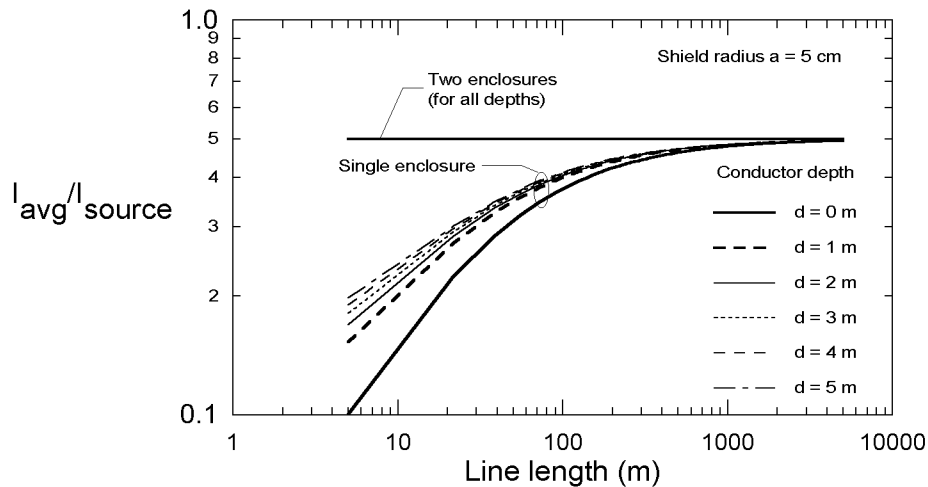


Figure 17. Plot of the average value of the late-time lightning current flowing onto the cable for a cable radius of 5 cm.

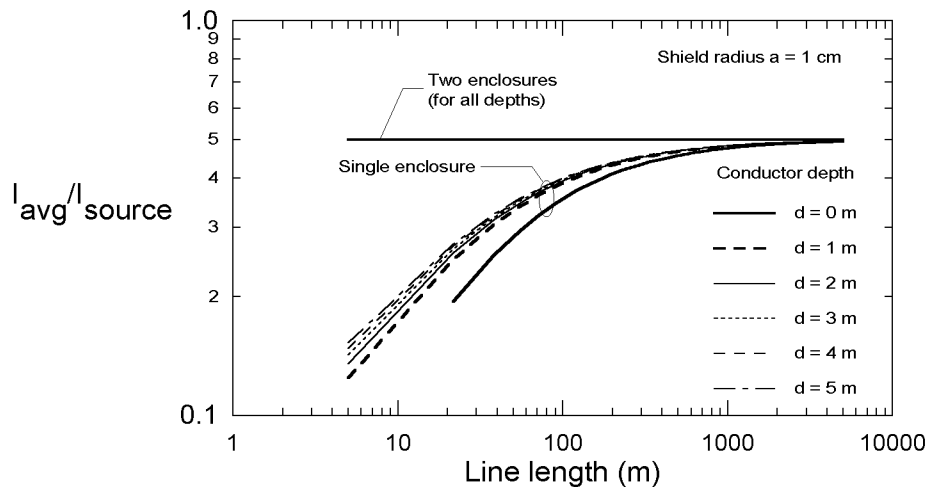


Figure 18. Plot of the average value of the late-time lightning current flowing onto the cable for a cable radius of 1 cm.

As a consequence of this examination of the lightning channel current splitting, it may be concluded that the late-time data in Figure 16 through Figure 18 should be used for estimating the current drive of buried cables directly excited by a lightning discharge. This is because of the fact that the late-time current splitting model is more appropriate for understanding the diffusion effects of the current through the cable shield. Moreover, because the current flowing on the shield at later times is larger than at early times, this model provides larger estimates of the internal responses, and thus leads to more conservative hardening requirements. This late-time current splitting model will be used in the next section for studies of the transient behavior of the currents flowing along the buried cable and the subsequent responses induced on internal wires.

4. Cable Coupling Model for Lightning Responses of Shielded Cables

For estimating the internal wire voltages within the cable shield of Figure 2, the idealized system geometry introduced in Figure 14 is first used to determine the current $I(x)$ flowing along the shield exterior. It is this current that provides the excitation to the signal wires inside the shield.

To determine the response of internal signal wires within the buried cable, a suitable cable shield model is needed. Reference [4] has discussed the two-region coupling problem illustrated in Figure 2, in which the external current on the shield interacts with the imperfectly conducting shield wall to produce a distributed voltage source on the inner walls of the shield. In this model, the internal signal wire is terminated in a constant load resistance R_L at each end of the line, and we are interested in evaluating the lightning-induced voltage at one of these loads.

Many practical shielded cables have multiple conductors within the shield. The analysis here assumes a single conductor and computes the wire-shield voltage (i.e., the common mode voltage). In the multiconductor case, it is possible to also have differential (wire-to-wire) voltages. However, the external lightning current on the shield tends to excite the common mode most strongly, and therefore, the details of a more general shielded multiconductor line are not pursued further here.

The cable shielding model developed in [4] was designed for very fast transients. As a consequence, the resulting expressions for the internal responses are rather complex. For the present case, however, considerable simplifications are possible due to the slow nature of the lightning waveform. As developed in Section 2, the lightning waveform has a characteristic duration time of several hundreds of milliseconds. This implies that for lines on the order of several km or shorter, the injected lightning current on the line need not be modeled as a traveling wave. A simple lumped parameter circuit model will suffice in this case.

Using the *transfer impedance* concept for the internal wire excitation [6], the distributed voltage source $V'_s(\omega)$ on the internal wire within the shield shown in Figure 3a is given by the expression

$$V'_s(\omega) = Z'_t(\omega)I(x) \quad , \quad (7)$$

where $I(x)$ is the shield current and $Z'_t(\omega)$ is a frequency-dependent transfer impedance of the shield which depends on both the shield geometry and the electrical properties of the shield material.

Because the line is assumed to be short compared with the wavelength $\lambda = c/f = 2\pi c/\omega$, all of the internal voltage sources can be summed together without taking into account transit time effects, and the simple equivalent circuit shown in Figure 3b results. In this expression, the lumped voltage source V_o is given by the integral of the distributed sources as

$$\begin{aligned}
V_o &= \int_0^L V'_s(x) dx = Z'_t \int_0^L I(x) dx \\
&= Z'_t L I_{avg}
\end{aligned} \tag{8}$$

where I_{avg} denotes the *average* shield current discussed earlier, and L is the line length. Once the voltage source V_o is determined, the induced lightning response at the load is simply given from Figure 3b by

$$V_L = V_o / 2. \tag{9}$$

In this report, we will be concentrating on the behavior of this load voltage. At times, however, the open-circuit voltage of the inner conductor V_{oc} may be of interest. This value is simply twice the load voltage:

$$V_{oc} = 2V_L = V_o \tag{10}$$

The ratio of the average current on the cable shield to the total injected lightning current has been determined previously and is given by the current splitting factor in Eq.(5). Thus, the internal load voltage at the equipment can be written as

$$V_L(\omega) = \frac{1}{2} Z'_t(\omega) \left(\frac{1/R_3 + 1/(2R_2)}{1/R_1 + 1/R_2 + 1/R_3} \right) L I_{source}(\omega). \tag{11}$$

Notice that this is essentially a frequency domain relationship, since the transfer impedance of the shield is defined as a function of the angular frequency ω . In the time domain, evaluating the load voltage requires the use of the *convolution* operation as

$$v_L(t) = \frac{fL}{2} z'_t(t) * I_{source}(t), \tag{12}$$

where $z'_t(t)$ is the inverse Fourier transform of the transfer impedance $Z'_t(\omega)$ and f is the bracketed term in Eq.(11).

5. Calculated Results for Lightning-Induced Cable Responses

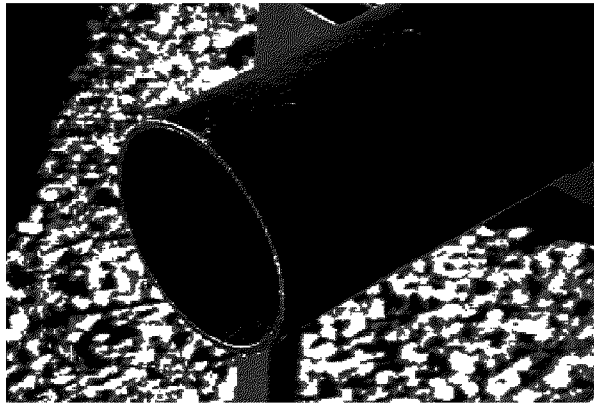
In this study, four different types of cable shields have been considered, and in this section we present a comparison of their effectiveness in protecting equipment from the lightning surges.

5.1 Cable Configurations

The first cable, denoted as the *version 1* cable, is an iron tube which can be welded at its joints to form a continuous shield. The second cable (the *version 2* cable) is a copper tube having corrugations that permit a degree of bending during installation, and the *version 3* cable is a Cr-Ni Steel shield having similar corrugations. Each of these cable shields is described by an average shield diameter d , the shield thickness Δ , the electrical conductivity of the shield material σ , and the relative magnetic permeability μ_r .

These three cable shields are in the form of a single highly conducting tube. The *version 4* cable is different, consisting of a two layer shield. The first shielding layer is a steel protective jacket, which offers both mechanical and electrical protection for the cable. The second layer is made of aluminum, and it provides additional electrical shielding. As a consequence, two sets of parameters d , Δ , σ , and μ_r are needed to describe this cable. Figure 19 illustrates the various cables, with the shields and internal wires clearly shown.

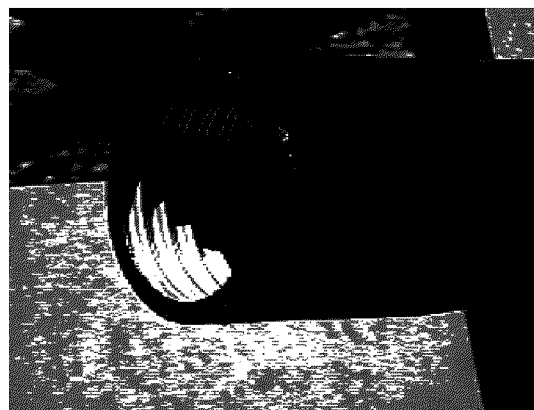
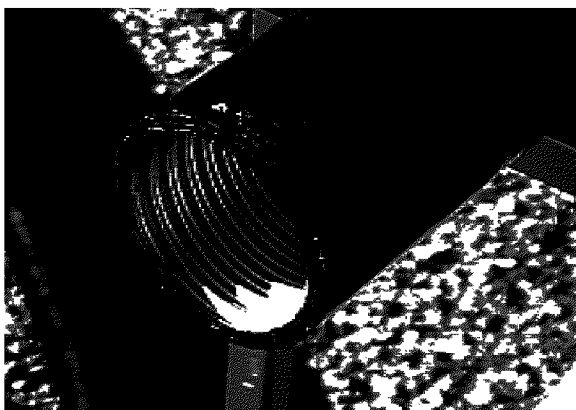
To summarize the cable parameters used for these calculations, Table 2 presents the pertinent shield data. Notice that for the corrugated cables, we assume that the nominal diameter of the tube is the average of the maximum and minimum radii. Furthermore, in the case of the Version 4 cables which have a steel cladding for protection, we assume that there are two electrical shields operating in parallel: one of steel with a high- μ value, and another of aluminum with a high conductivity.



(a) Version 1: Steel tube shield

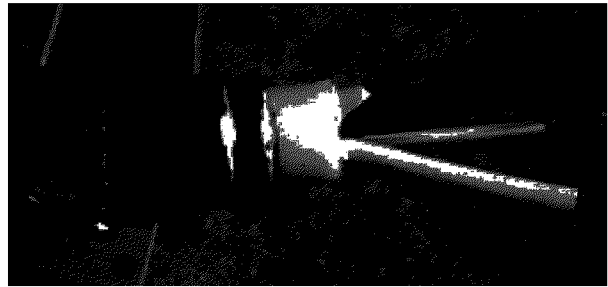


(b) Version 2: Corrugated copper shield

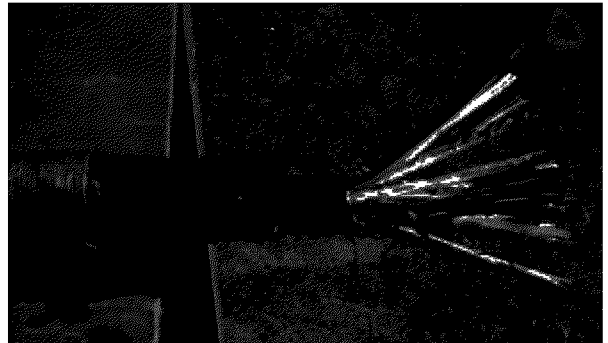
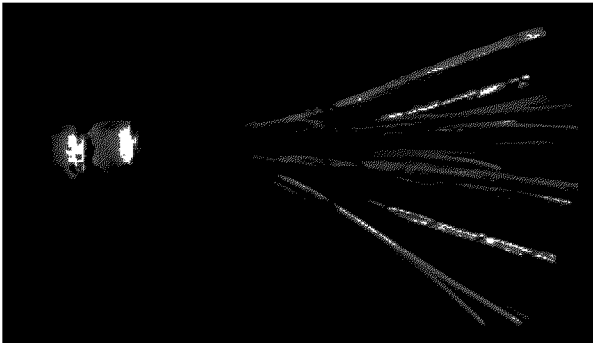


(c) Version 3: Corrugated Cr-Ni steel shield (two views)

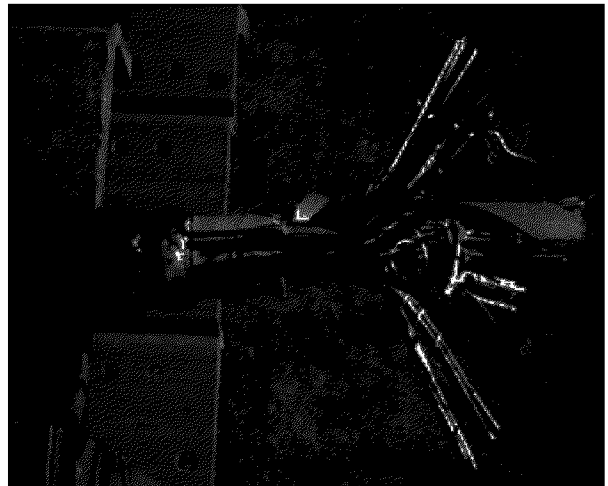
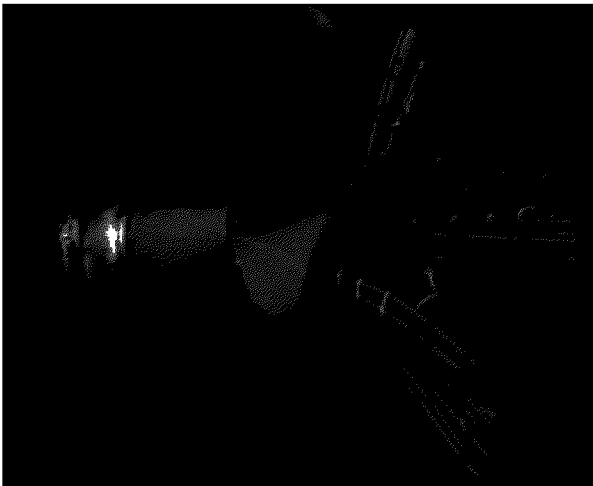
Figure 19. Photographs of the shielded cables.



(d) Version 4: Power cable



(e) Version 4: Signal cable



(f) Version 4: Special cable

Figure 19. Photographs of the shielded cables. (Concluded)

Table 2 Electrical parameters and dimensions for the cable shields

	Version 1 cable	Version 2 cable	Version 3 cable	Version 4 (power cable)	Version 4 (signal cable)	Version 4 (special cable)
Protective Covering layer	None	None	None	None	None	None
Average Diameter d (mm)	---	---	---	46	46	46
Thickness Δ (mm)	---	---	---	1.2	1.2	1.2
σ (S/m)	---	---	---	5.51×10^6	5.51×10^6	5.51×10^6
μ_r						
EM Shield layer	Iron	Copper	Co-Ni Steel	Al	Al	Al
Average Diameter D (mm)	85.7	66.5	84	33.75	33.0	27.5
Thickness Δ (mm)	3.2	0.6	0.6	1.4	1.4	1.4
σ (S/m)	5.51×10^6	5.8×10^7	1.1×10^6	3.96×10^7	3.96×10^7	3.96×10^7
μ_r	2000	1	1	1	1	1

5.2 Transfer Impedance of Cable Shields

The transfer impedance of a tubular shield has been discussed in Section 9.3.1 of ref.[4]. For a single shield with diameter d , and thickness Δ , the transfer impedance is defined as

$$Z'_t(\omega) = R'_{dc} \frac{(1+j)\Delta/\delta}{\sinh((1+j)\Delta/\delta)} \quad (\Omega/\text{m}) \quad (13)$$

where R'_{dc} is the static per-unit-length resistance of the shield, given by

$$R'_{dc} = \frac{1}{\pi \sigma d \Delta} \quad (\Omega/\text{m}) \quad (14)$$

and δ is the electrical skin depth in the material, expressed as

$$\delta = \sqrt{\frac{2}{\omega \sigma \mu_r \mu_o}} \quad (\text{m}), \quad (15)$$

where ω is the angular frequency, σ is the conductivity, and the quantity $\mu_r \mu_o$ is the shield magnetic permeability.

For the two-shield cable, Vance [6] describes a more complex relationship for the transfer impedance. This is

$$Z'_t(\omega) = \frac{R'_{dc1} R'_{dc2} \frac{(1+j)\Delta_1/\delta_1}{\sinh((1+j)\Delta_1/\delta_1)} \frac{(1+j)\Delta_2/\delta_2}{\sinh((1+j)\Delta_2/\delta_2)}}{R'_{dc1} ((1+j)\Delta_1/\delta_1) \coth((1+j)\Delta_1/\delta_1) + R'_{dc2} ((1+j)\Delta_2/\delta_2) \coth((1+j)\Delta_2/\delta_2)} \quad (15)$$

where the subscripts 1 or 2 denote the appropriate parameters for the first or second shield layer.

As an example of the behavior of the transfer impedances, Figure 20 plots the calculated transfer impedance magnitude $|Z'_t|$ for cable versions 1, 2, and 3 as a function of frequency. Notice that the steel pipe (version 1) provides the best shielding at the higher frequencies, due to the high permeability. However, at low frequencies, its shielding is not as good as the copper tube (version 2), due to its higher electrical conductivity. Cable version 3 (the Cr-Ni steel tube) is not a very good shield, due to its relatively low conductivity.

The composite cable (Version 4) is different, in that it has two shields. Each shield will attenuate the EM fields, and the total shielding of the cable is found by a suitable combination of the two. Figure 21 presents the transfer impedance magnitudes for the isolated steel liner, for the isolated aluminum shield, and for the combined shields. Notice that there are slight differences in the aluminum shield diameters in each of the version 4 cables of Table 2, and this accounts for the very small differences in the curves in Figure 21.

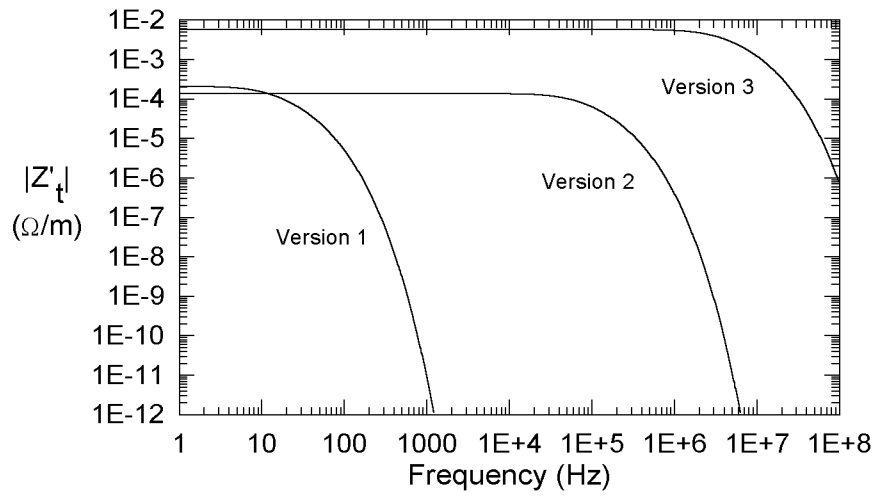


Figure 20. Plot of the transfer impedance $|Z'_t|$ for cable versions 1, 2, and 3.

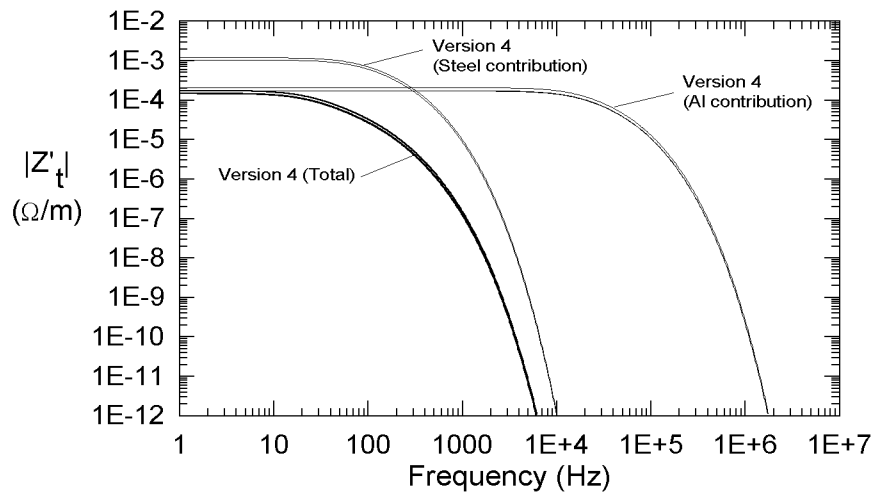


Figure 21. Plots of the transfer impedance $|Z'_t|$ for cable versions 4.

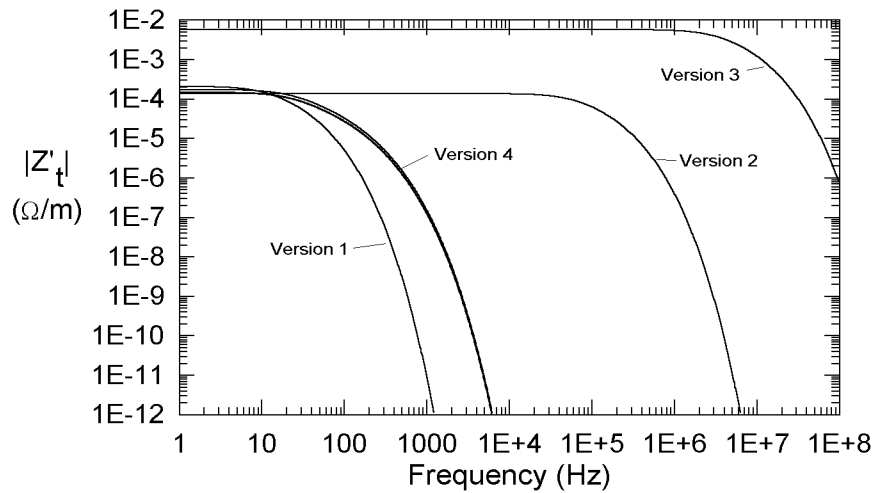


Figure 22. Comparison of $|Z'_t|$ for all cables.

To compare the shielding of the four cables, Figure 22 plots $|Z'_t|$ for all cables together on the same diagram. At low frequencies, $|Z'_t|$ becomes purely resistive and the DC values computed for the cables are summarized in Table 3. Also shown in this table are the corresponding measured values¹. Agreement between the theoretical and numerical results is reasonable.

Table 3. DC per-unit-length resistance values for the various cable shields.

Cable Configuration	Calculated DC per unit length Resistance mΩ/m	Measured DC per unit length Resistance mΩ/m
Version 1	0.21	0.16
Version 2	0.14	0.19
Version 3	5.74	6.07
Version 4 (power)	0.15	0.20
Version 4 (signal)	0.15	Not measured
Version 4 (special)	0.18	0.21

5.3 Internal Voltage Responses

With the transfer impedances of the cables defined and a model for the coupling mechanisms of the lightning current developed, it is possible to estimate the lightning induced cable responses for the shields. To have a consistent excitation function for all cases, the *normalized* lightning waveform $g(t)$ shown in Figure 23 is assumed. The lightning transient excitation current is then expressed as

$$I_{source}(t) = I_o g(t), \quad (17)$$

where the amplitude I_o is chosen to be 50 kA. The corresponding spectral magnitude of the normalized waveform function $g(\omega)$ is shown in Figure 7, if the curve is scaled by a factor of 50,000.

¹

Measured results were provided by Prof. M. Ianoz of the EPFL in Lausanne.

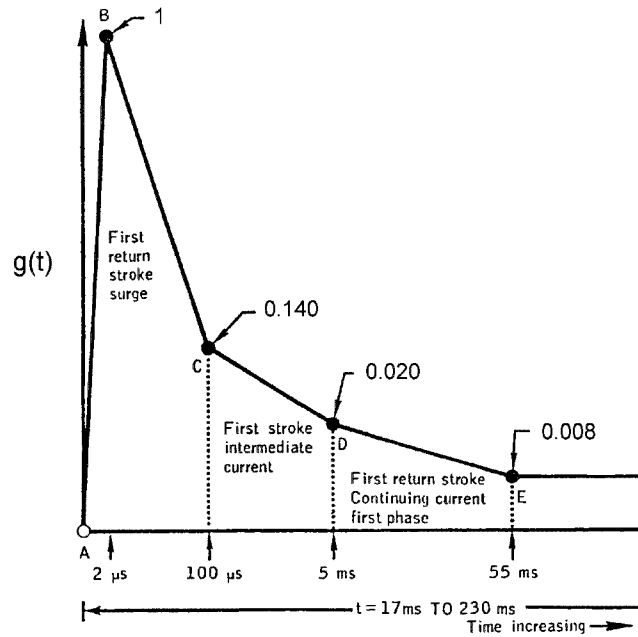


Figure 23. Normalized lightning waveform $g(t)$.

5.3.1 Responses for cable shield versions 2 and 3

In comparing the excitation spectrum of the lightning in Figure 7 with the spectra of the transfer impedances shown in Figure 20, we see that for the version 2 and 3 shields the transfer impedances of the shields are virtually constant over bandwidth of the excitation function. Thus, the transfer impedance in Eq.(11) may be approximated by its dc resistive value, and the internal transient load voltage is evaluated simply as

$$v_L(t) = \frac{fL}{2} R'_{dc} I_o g(t). \quad (18)$$

Note that the time history of the internal voltage responses for these cases is identical with that of the external lightning waveform.

Figure 24 and Figure 25 illustrate the peak values of the internal load voltages for these versions of the shielded cable. Cable version 3 is the poorest shield, and for a 1 km line length internal voltages approaching 100 kV are noted. Cable version 2 is a better shield, with a peak voltage of about 1 kV for the 1 km line. This enhanced shielding is due entirely to the higher conductivity of the shield material.

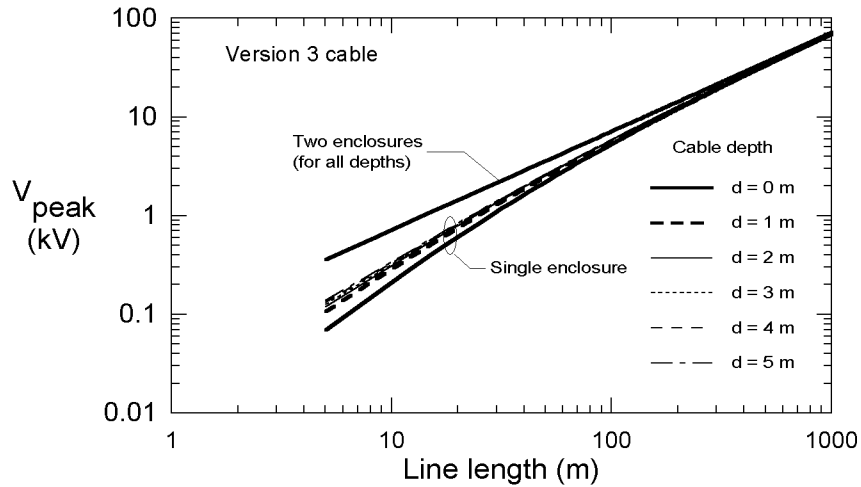


Figure 24. Plot of the peak load voltage inside the version 3 shielded cable as a function of line length and system configuration.

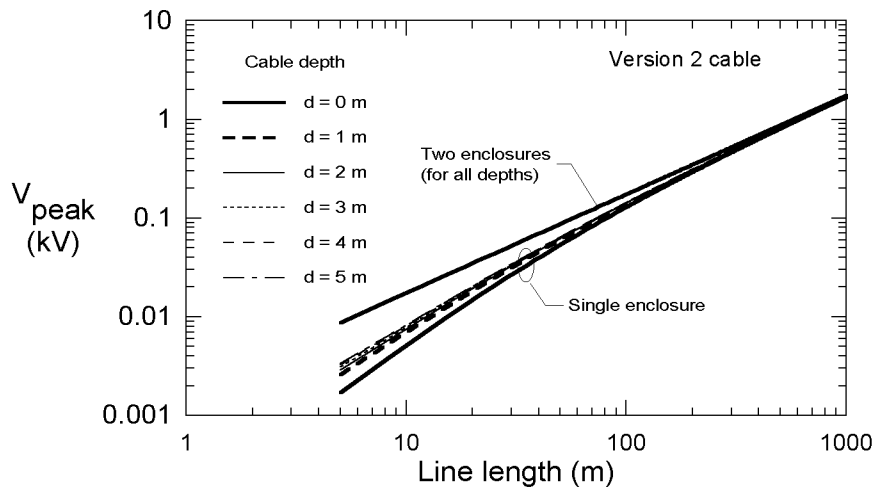


Figure 25. Plot of the peak load voltage inside the version 2 shielded cable as a function of line length and system configuration.

5.3.2 Responses for cable shield version 1

Version 1 of the shielded cable offers the best protection, due to its relatively high conductivity and to the high- μ magnetic properties which causes a rather fast high-frequency increase in the shielding. Unfortunately, because the frequency domain spectrum of the transfer impedance changes appreciably over the same frequency range as the excitation spectrum, the evaluation of the convolution in Eq.(12) must be evaluated carefully.

The inverse Fourier transform of the transfer impedance of the version 1 cable of Figure 20 provides the impulse response of the shield $z'_t(t)$. This is illustrated in Figure 26. For comparison, the other impulse responses for cable versions 2 and 3 were delta functions in time, with a weight equal to the dc per-unit-length shield resistance. Thus, the effect of the version 1 shield is to broaden the excitation pulse in time.

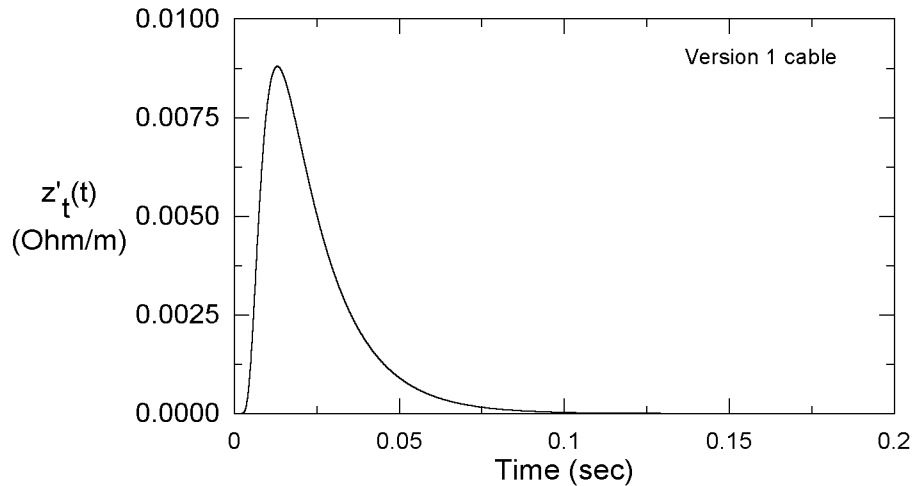


Figure 26. Plot of the impulse response of the version 1 cable shield transfer impedance.

The evaluation of the internal response for this shielded cable requires the evaluation of the convolution operator in Eq.(12), using the functions in Figure 23 for $g(t)$ and Figure 26 for $z'_t(t)$. The resulting waveform, which is essentially the time history of the internal voltage response, is shown in Figure 27. Figure 28 plots the corresponding peak internal load voltages on this cable for the various system configurations. Notice that the shielding for this cable is significantly better than the others, with a peak voltage of about 100 V for the 1000 m line.

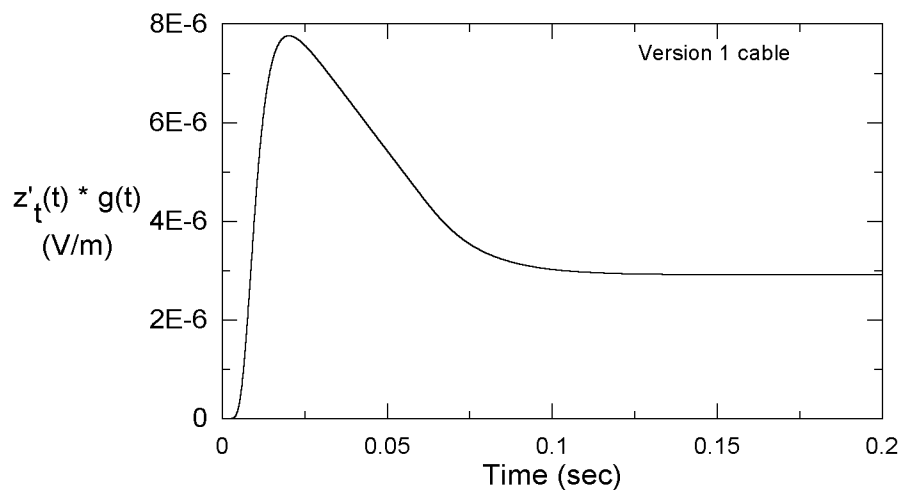


Figure 27. Plot of the internal response waveform resulting from the convolution of $z'_t(t)*g(t)$ for cable shield version 1.

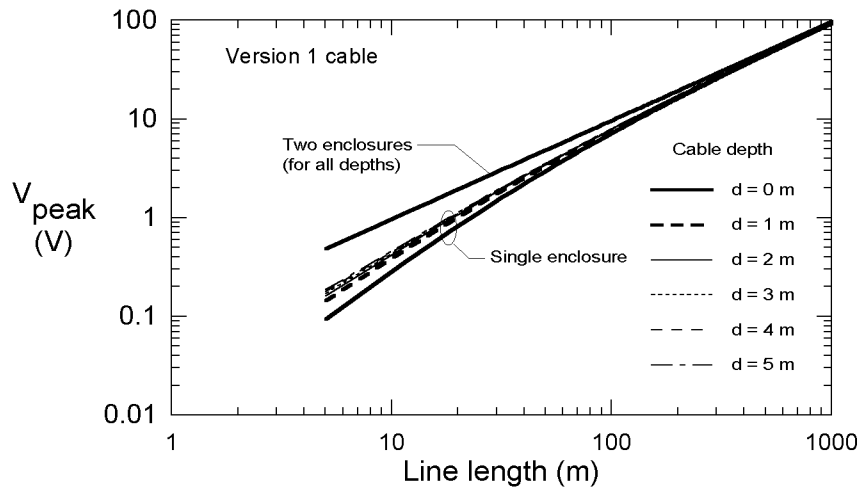


Figure 28. Plot of the internal peak voltage response for the version 1 cable shield. (Note the ordinate scale is in volts.)

5.3.3 Responses for cable shield version 4

The cable with shield version 4 is similar to version 1, in that the transfer impedance spectrum changes significantly within the bandwidth of the excitation spectrum, and the convolution operation of Eq.(12) must be computed to find the internal wire voltage. For the spectrum of the transfer impedance for this shield, Figure 29 presents the impulse response $z'_t(t)$ and the resulting convolution waveform is shown in Figure 30. Notice that this latter waveform is more like the driving lightning waveform, due to the higher frequency content in the transfer impedance than was encountered for the version 1 shield.

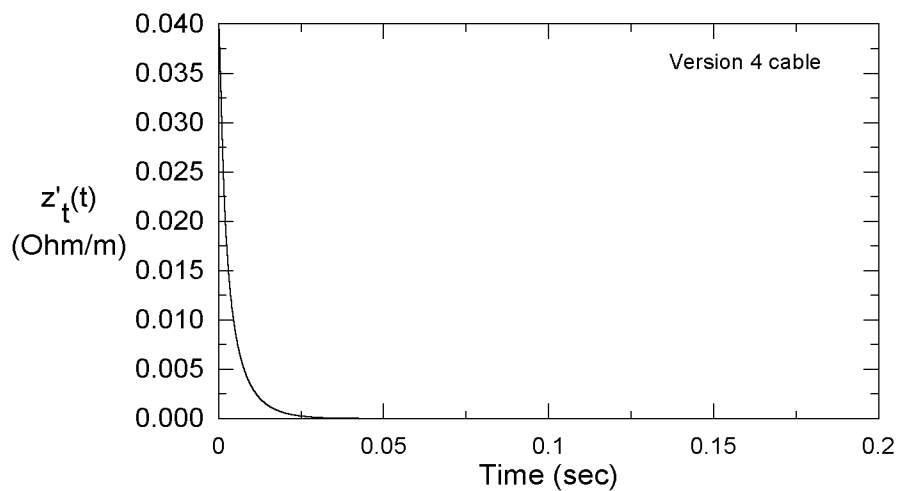


Figure 29. Plot of the impulse response of the version 4 cable shield transfer impedance.

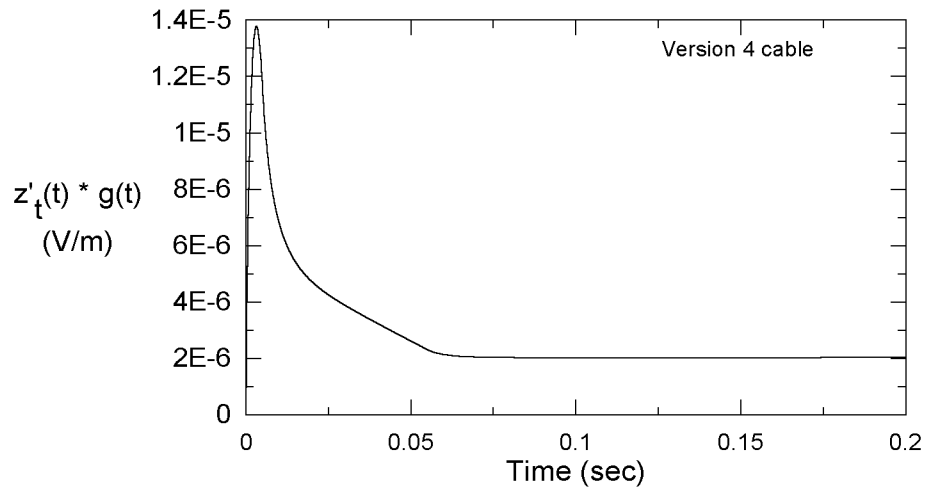


Figure 30. Plot of the internal response waveform resulting from the convolution of $z'_t(t)*g(t)$ for cable shield version 4.

For this shield, Figure 31 plots the maximum peak internal wire voltage for the different system configurations and as a function of the cable length. Note that this response is about a factor of 2 higher than the best shielding case (the version 1 cable)

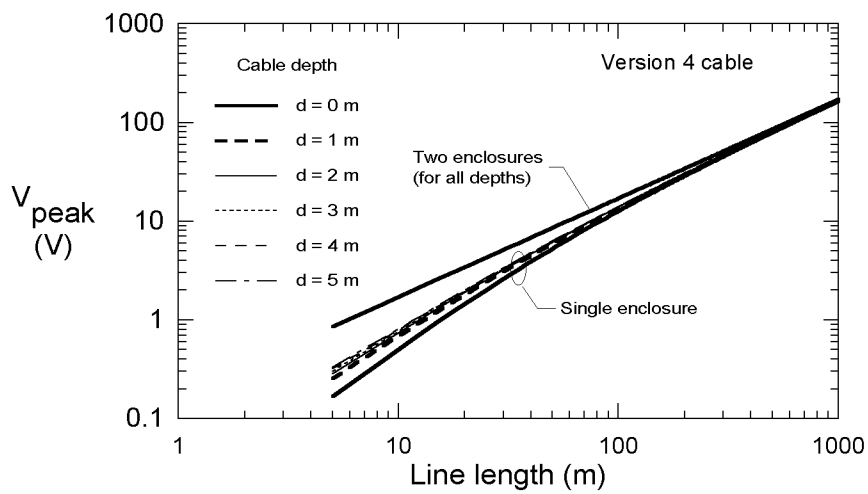


Figure 31. Plot of the internal peak voltage response for the version 4 cable shield. (Note the ordinate scale is in volts.)

6. Summary

It is clear that the version 1 cable offers the best protection. This is due to the magnetic effects of the shield. Because the version 4 shield also has a slight amount of magnetic material in the form of a protective steel wire layer, this latter cable also provides a reasonable amount of shielding and protection against the lightning surge. The version 2 cable offers a smaller amount of shielding, and the version 3 cable is the worst, due to its relatively low electrical conductivity.

To summarize the expected load voltage surges induced by a direct lightning strike of the system, Table 4 presents the peak values of the voltage, the rates of rise, and the 50% fall times for the four cable shield versions, assuming a 1 km line length. Given the nature of internal electronics equipment, these data will assist in defining the necessary lightning protection requirements.

Table 4. Summary of lightning-induced voltage surge characteristics for a 1 km buried line.

Cable Shield Type	Peak Voltage kV	Rate of Rise kA/μs	50% Fall time
Version 1	0.1	5.0×10^{-6}	62.3 ms
Version 2	2.0	1.0	61.0 μs
Version 3	70.0	35.0	61.0 μs
Version 4	0.2	6.5×10^{-5}	9.9 ms

7. References

1. Fisher, F.A, et. al., **Lightning Protection of Aircraft**, Lightning Technologies, Inc., Pittsfield, MA, 1990.
2. Anderson, R.B., and A.J. Ericksson, “Lightning Parameters for Engineering Applications”, *Electra*, Vol. 69, pp.65-102.
3. Kunz, K. S, and R. Leubbers, **The Finite Difference Time Domain Method**, CRC Press, 1994.
4. Tesche, F. M., et. al., **EMC Analysis Methods and Computational Models**, John Wiley and Sons, New York, December 1996.
5. Sunde, E.D., **Earth Conduction Effects in Transmission Systems**, D. Van Nostrand Co., Inc, New York, 1949.
6. Vance, E.F., **Coupling to Shielded Cables**, Krieger Press, Melbourne, FL, 1987.

Appendix A

Description of an Alternate Lightning Environment

A different lightning channel current model has been recently used in ref.[A1], and is discussed in ref.[A2] Unlike the piece-wise linear waveform of Figure 6, this alternate environment has an analytic representation of the transient current. It is expressed by a *sum* of two functions, each of the form

$$i(t) = \frac{I_o}{\eta} \frac{(t/\tau_1)^n}{1 + (t/\tau_1)^n} e^{-t/\tau_2}, \quad (A1)$$

where η is an amplitude normalization factor defined as

$$\eta = e^{-\left[(\tau_1/\tau_2)(n\tau_2/\tau_1)^{(1/n)}\right]}, \quad (A2)$$

so that the peak value of the transient waveform is I_o . The parameters required for the two functions to resemble a measured lightning return current waveform are summarized in Table A1, with the resulting transient current waveform and its Fourier spectrum shown in Figures A1 and A2, respectively.

Table A1. Parameters for representing the current waveform at the base of a lightning channel.

Waveform	I (kA)	τ_1 (μ s)	τ_2 (μ s)	n
1	10.7	0.25	2.5	2
2	7.5	2.1	2.30	2

¹. Nucci, C. A., and F. Rachidi, "Experimental Validation of a Modification to the Transmission Line Model for LEMP Calculations", **Proc. 8th Int. Symposium and Technical Exhibition on EMC**, Zurich, Switzerland, arch 1989, pp. 389-394.

². Tesche, F. M., et. al., **EMC Analysis Methods and Computational Models**, John Wiley and Sons, New York, December 1996.

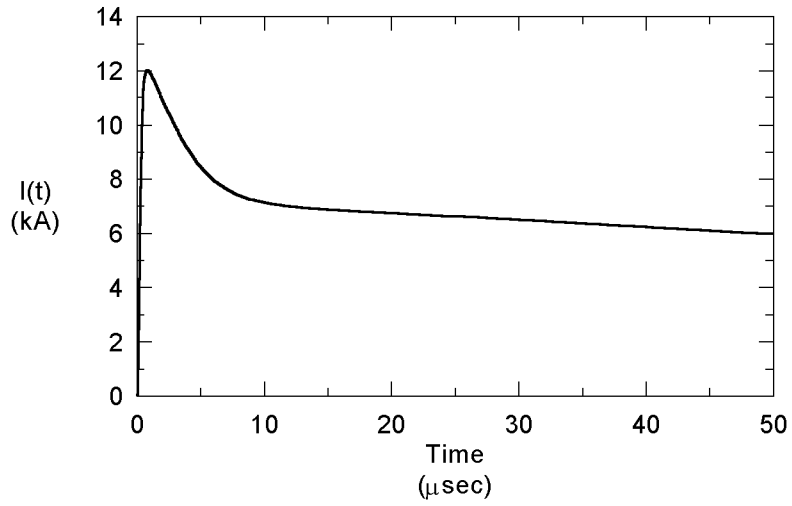


Figure A1. An alternate lightning current specification from [1].

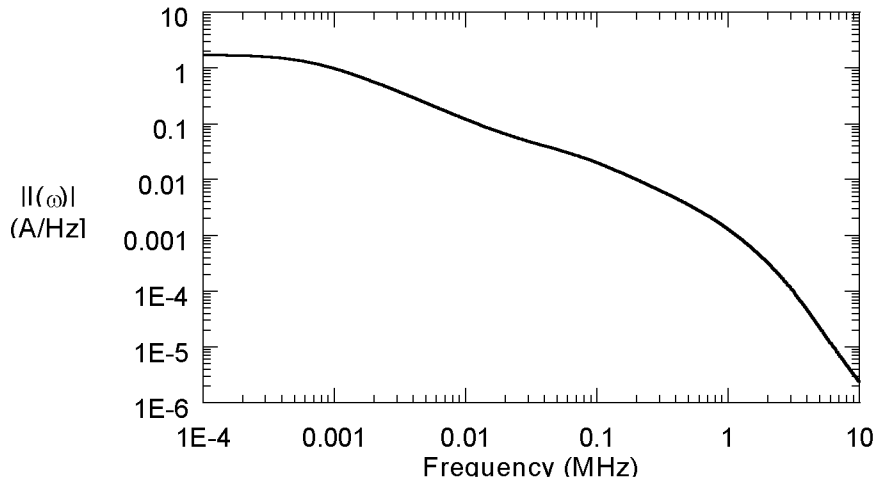


Figure A2. Lightning current spectral magnitude for the waveform of Figure A1.